This manuscript has been accepted for publication in Palaeogeography, Palaeoclimatology, Palaeoecology. Please refer to the published version at https://doi.org/10.1016/j.palaeo.2021.110550

Early Pleistocene integration of the Yellow River II: Evidence from the Plio-Pleistocene sedimentary record of the Fenwei Basin

Guoqiao Xiao[a, b, d, *], Qing Pan[a], Qingyu Zhao[b], Qiuzhen Yin[c], Ruisheng Chen[a], Hong Ao[b, d], Xinxia Li[a], Zongmin Zhu[b]

[a] *Hubei Key Laboratory of Critical Zone Evolution, School of Geography and Information Engineering, China University of Geosciences, Wuhan 430074, China*

[b] *State Key Laboratory of Biogeology and Environmental Geology, School of Earth Sciences, China University of Geosciences, Wuhan 430074, China*

[c] *Georges Lemaître Centre for Earth and Climate Research, Earth and Life Institute, Université Catholique de Louvain, Louvain-La-Neuve, 1348, Belgium*

[d] *State Key Laboratory of Loess and Quaternary Geology, Institute of Earth Environment, Chinese Academy of Sciences, Xi'an 710061, China*

* Corresponding author
E-mail address: xgqiaocug@gmail.com or gqxiaocug@126.com

Abstract

The Yellow River is the 2nd longest river in China and the 6th longest river in the world. However, the timing and mechanism of its integration remains debated. During the establishment of its present geometry, the Yellow River captured and deeply incised into a series of local drainage basins along its Upper and Middle Reaches. The termination of basin filling, therefore, can be linked to the development of the Yellow River. The Sanmen paleolake, a Plio-Pleistocene endorheic mega-lake situated in the Fenwei Basin, was the last catchment basin captured by the Yellow River before it emptied into the sea. The final termination of the lacustrine deposition in the Fenwei Basin can therefore indicate the integration of the Yellow River. Here, we present the results of a detailed magnetostratigraphic and magnetic susceptibility study of a lacustrine-loess section from the southeastern part of the Fenwei Basin (Sanmenxia Subbasin), and aim to (1) explore the sedimentary evolution of the Sanmen paleolake and refine the age of the Sanmen Formation in this area, and (2) investigate the precise timing of the integration of the Yellow River. Our results show that the Sanmenxia Subbasin was occupied by a salty lake between 2.7 and 2.2 Ma, then it gradually changed to an alternation of shallow lake and floodplain environments between 2.2 and 1.6 Ma, and it finally irreversible dried up at ~1.6 Ma and was subsequently covered by loess-paleosol sequences. The drying up of the Sanmen paleolake at ~1.6 Ma indicated the establishment of the connection between the Middle and Lower Reaches of the Yellow River.

Keywords: Quaternary; Sanmen Paleolake; Sanmen Formation; loess; paleomagnetism; river capture

1. Introduction

With the length over 5,400 km, the Yellow River (Huanghe in Chinese) is the 2nd longest river in China and the 6th longest river in the world. The Ω shape of the Yellow River (Fig. 1) suggests that its evolution history is complex. Previous investigations demonstrated that the Yellow River achieved its present shape by integrating a series of separated local drainage basins along its Upper and Middle Reaches (Zhu, 1989; Craddock et al., 2010; Xiao et al., 2020). These basins along its main course include the Fenwei, Hetao, Yinchuan, Linxia, Guide, Xunhua, Gonghe, Tongde, and Zoige Basins (Fig. 1). The termination of basin filling and changing to an exorheic drainage have been attributed to the development of the modern Yellow River (Craddock et al., 2010; Bridgland et al., 2020). Based on the age of the youngest lacustrine sediments in the Linxia (Fang et al., 2003), Guide (Fang et al., 2005), and Tongde Basins (Craddock et al., 2010), previous studies suggested a rapid integration of the Upper Reaches of the Yellow River since ~1.7 Ma (Craddock et al., 2010). However, disagreement still exists on the age of the youngest lacustrine sediments in the Fenwei Basin, with estimates ranging from ~1.9 to ~0.15 Ma (e.g., Yue, 1996; Han et al., 1997; Wang et al., 1999, 2002a, 2002b; Li et al., 2004; Kong et al., 2014), which allows the possibility that integration of the Yellow River began more recently. This is because the Fenwei Basin is the last catchment basin before the Yellow River empties into the sea, and only when it becomes an exorheic drainage will it indicate the integration of the Yellow River.

[Figure 1]

With an average elevation over 400 m and area over 35, 000 km^2, the Fenwei Basin is situated in the Middle Reaches of the Yellow River (Fig. 1). The basin contains four subbasins (Fig. 2), including the Weihe, Yuncheng, Linfen, and Sanmenxia Subbasins (Zhang et al., 1998; Shi et al., 2019). The southeastern part of the Fenwei Basin (i.e., Sanmenxia Subbasin) is separated from the low-elevation (<50 m) North China Plain in the Lower Reaches of the Yellow River by the ~100 km-wide Xiaoshan Mountain uplift block (belongs to the southern part of the Taihang Mountains). Investigations have demonstrated that a Plio-Pleistocene endorheic mega-lake, the Sanmen paleolake, situated in the Fenwei Basin (Wang et al., 1982, 2002a; Liu et al., 2006). As the elevation of the Sanmen paleolake is ~300 m higher than the North China Plain, this paleolake would be drained and deeply incised when the Yellow River cut through the Xiaoshan Mountain. Indeed, numerous investigations have shown that the widespread lacustrine deposition in the Sanmen paleolake disappeared in the early Pleistocene and was followed by loess-paleosol sequences (e.g., Yu et al., 1982; He et al., 1984; Sun et al., 1988; Ge et al., 1991; Yue, 1996; Han et al., 1997; Wang et al., 2002a; Li et al., 2004; Tan et al., 2011; Kong et al., 2013, 2014; Qiu et al., 2018). After that, only several separated small endorheic salty lakes remain in the Fenwei Basin, such as the Yuncheng salty lake within the Yuncheng subbasin (Wang et al., 2002a; Yan et al., 2020) and the

Luyang salty lake within the Weihe subbasin (Rits et al., 2016), indicating the demise of the Sanmen paleolake. Therefore, the disappearance of the lacustrine deposition and occurrence of loess-paleosol sequences in the Fenwei Basin can be the indicator of integrating the Middle and Lower Reaches of the Yellow River.

[Figure 2]

However, debate still exists on the timing of the demise of the Sanmen paleolake. Based on the sedimentary record from the Huangdigou section (see Fig. 2a for location) in the eastern part of the Sanmenxia Subbasin, some researchers suggested that the Sanmen paleolake irreversible dried up at ~0.15 Ma, and proposed that the Yellow River established at ~0.15 Ma (Wu et al., 1998; Wang et al., 1999; Wang et al., 2002b; Jiang et al., 2007). In addition, the loess deposits at Mangshan section from the North China Plain displayed a pronounced increase in sedimentation rates and grain-size between 0.24 and 0.15 Ma (Jiang et al., 2007; Zheng et al., 2007). As these loess materials were sourced from the lower Yellow River floodplain, some proposed that the Sanmen paleolake was captured by the Yellow River during 0.24–0.15 Ma (Jiang et al., 2007; Zheng et al., 2007). In contrast, other lines of evidence suggested an earlier integration of the Yellow River. Numerous investigations from the Weihe, Yuncheng, and Linfen Subbasins demonstrated that the lacustrine deposition changed to loess-paleosol sequences occurred between 1.9 and 1.2 Ma (e.g., Yu et al., 1982; He et al., 1984; Sun et al., 1988; Ge et al., 1991; Yue, 1996; Han et al., 1997; Wang et al., 2002a; Li et al., 2004; Tan et al., 2011; Kong et al., 2013, 2014; Qiu et al., 2018). Further, the ages of the regional planation surface and the uppermost terrace along the Sanmenxia Subbasin and Sanmen Gorge suggested that the Sanmen paleolake was captured by the Yellow Rive during 3.6-1.2 Ma (Kong et al., 2014; Hu et al., 2017). In addition, provenance studies from sedimentary cores in the Lower Yellow River suggested that the onset of input of materials from the Chinese Loess Plateau into the Lower Yellow River occurred between 1.6 and 0.8 Ma (Yao et al., 2017; Zhang et al., 2019; Xiao et al., 2020), indicating that the Sanmen paleolake was captured during this interval.

In order to further determine the exact timing of the integration of the Yellow River, in this study, we report the results of a detailed magnetostratigraphic and magnetic susceptibility study of a lacustrine-loess succession from the Zhangcun section in the Sanmenxia Subbasin. Our magnetostratigraphic results provide reliable chronostratigraphic frameworks for the upper Pliocene-Pleistocene sediments in the Sanmenxia Subbasin, enabling us to reassess the previous results from the Huangdigou section in this basin and precisely estimate the timing of integration of the Yellow River.

2. Geological setting and Cenozoic stratigraphy

The studied Sanmenxia Subbasin is a W–E elongate basin (Fig. 2a), which is about 120 km in length, 20–30 km in width, with an area of ~3100 km^2. The Sanmenxia Subbasin lies between the Huashan Mountains to the south and the Zhongtiaoshan Mountains to the north. Due to the far-field effect of initial India–Asia continental collision, significant exhumation and uplift of the Huashan and Zhongtiaoshan

Mountains resulted in extension and formation of the Sanmenxia graben basin in early Cenozoic (Han et al., 2002; Liu et al., 2013; Shi et al., 2019), with the Cenozoic deposits over 4000 m in thickness (Fig. 2b).

The Paleogene strata of the Sanmenxia Subbasin, the Pinglu Group, are well exposed near the Sanmenxia reservoir (Fig. 3h), with a thickness over 1000 m. Recent geological surveys revealed that the base age of the Pinglu Group is ~65 Ma (Zhu et al., 2008), and it unconformably underlain by the coal-bearing strata of Permian–Carboniferous. Lithological and biostratigraphic investigations suggested that the Pinglu Group was consist of purple basal conglomerates, overlain by red sandstones and mudstones (Fig. 3h), intercalated with green gypsiferous mudstones, indicating they were accumulated under arid alluvial plain and shallow lake environments (Zhu et al., 2008). According to the ESR dating, the Paleogene lithostratigraphic units in this area were further divided into the Batou (65–56 Ma), Menli (56–50 Ma), Podi (50–42 Ma), Zhaojialing (42–39 Ma), Xitan (39–33 Ma), Xiaoan (33–31 Ma), and Liulinhe (31–23 Ma) Formations (Zhu et al., 2008).

[Figure 3]

The Neogene strata of the Sanmenxia Subbasin are only partly exposed at the Huangdigou section near the east edge of the basin, which were unconformably underlain by the Paleogene Pinglu Group (Wang et al., 1999; Jiang et al., 2007). However, their contact relationship in the depocenter of the basin is still unknown. Our lithological investigations suggested that the lower part of the Huangdigou section mainly consists of interbed pale reddish calcareous siltstones and reddish-brown paleosol horizons, intercalated with fluvial sandstone and conglomerates (Fig. 3g), indicating that they were the depositions of active channels, sheet floods, and floodplains with paleosols in semiarid alluvial plain environments. These lithological characteristics were very similar to the upper Miocene Bahe Formation in the Weihe Subbasin (Kaakinen and Lunkka, 2003; Wang et al., 2014). The upper part of the Huangdigou section was mainly consist of pale yellow huge-thick lenticular sandstone intercalated with green-grayish calcareous mudstone (Fig. 3f), indicating a fluvial-lacustrine environment. These lithological characteristics were very similar to the Pliocene Youhe Formation in the Weihe Subbasin (Xue, 1981; Yue, 1996; Han et al., 1997; Liu and Xue, 2004). The Youhe Formation is widely exposed along the valleys of Weihe River and Yellow River in the Weihe and Sanmenxia Subbasins, and also can be observed in the studied Hougou subsection (Fig. 3d). Magnetostratigraphic and mammalian fossil investigations from the Weihe Subbasin suggested that the age of the Youhe Formation was between 3.4 and 2.6 Ma (Xue, 1981; Yue, 1996; Han et al., 1997; Liu and Xue, 2004). This stratigraphic correlation for the Huangdigou section is supported by the biochronologic investigation from this section, which suggested that it may span from late Miocene to early Pleistocene (Yuan, 1986).

The Youhe Formation was overlain by the famous Sanmen Formation, a representative of terrestrial lithostratigraphic unit in Northern China (Deng et al., 2019) that has been investigated over a century (Andersson, 1923). Magnetostratigraphic investigations from the Weihe Subbasin suggested that the basal age of the Sanmen Formation was ~2.6 Ma (Yue, 1996; Liu and Xue, 2004). The Sanmen Formation can be lithologically divided into two parts. The lower part consists of interbed pale yellow siltstone and green-grayish calcareous mudstone, indicating alternations of deep and shallow lacustrine environments. This part of strata is widespread in the Fenwei Basin and can be easily identified in our study section (Fig. 3c). According to previous reports of the lower Sanmen Formation (Yu et al., 1982; He et al., 1984; Sun et al., 1988; Ge et al., 1991; Yue, 1996; Wang et al., 2002a; Hu et al., 2005; Tan et al., 2011; Kong et al., 2013; Rits et al., 2016; Qiu et al., 2018; Shi et al., 2019; Yan et al., 2020), we can reconstruct the approximate area of the Sanmen Paleolake during this period (Fig. 2a). The upper part of the Sanmen Formation mainly consists of interbed pale-yellow calcareous siltstones and reddish-brown paleosol horizons (Figs. 3b–e), intercalated with fluvial conglomerate lens, indicating alternations of shallow lake and floodplain environments. The paleosol layers in the upper of the Sanmen Formation can be correlated to loess-paleosol sequences of Chinese loess (Figs. 3b–c), and these strata were called the water-reworked loess, which is very common in the basins within the distribution area of the Chinese loess (Liu, 1985), such as the Tianshui Basin (Wang et al., 2017), Fenwei Basin (Liu, 1985), and Nihewan Basin (Xia, 1992). Micropaleontological investigations demonstrated that some non-marine foraminiferal fauna and brackish ostracods in the Youhe and Sanmen Formations (Wang et al., 1982; Wang et al., 2002a), indicating that the Sanmen paleolake was once a salty lake. This was further supported by the later paleosalinity reconstructions from the Youhe and

Sanmen Formations (Liu et al., 2006). These lines of evidence suggested that the Fenwei Basin was an endorheic basin before the integration of the Yellow River.

The fluvial-lacustrine sequences of the Sanmen Formation in the Fenwei Basin were widely replaced by the loess-paleosol sequences since the early Pleistocene (He et al., 1984; Yue, 1996; Wang et al., 2002a; Li et al., 2004; Qiu et al., 2018), indicating the finally dried up of the Sanmen paleolake. Many magnetostratigraphic investigations from the Weihe and Yuncheng Subbasins suggested that the end of the Sanmen Formation varied between 1.9 and 1.2 Ma (Sun et al., 1988; Ge et al., 1991; Yue, 1996; Han et al., 1997; Wang et al., 2002a; Li et al., 2004; Qiu et al., 2018), albeit some discrepancies still existed among different sites. However, the magnetostratigraphic studies at the Huangdigou section from the Sanmenxia Subbasin suggested that the end of the Sanmen Formation was at ~0.15 Ma (Wang et al., 1999; Jiang et al., 2007). In this study, we will focus on the age of the Sanmen Formation in the Sanmenxia Subbasin.

3. Materials and methods

3.1. Studied geological section

The studied Zhangcun section is located at Zhangcun Town, Pinglu County, Shanxi Province (Fig. 2a). The section lies in the easternmost part of the Sanmenxia Subbasin, and thus an ideal site to investigate the evolution of the Sanmen paleolake. The composite Zhangcun section consists of the Guanjiawo (34°50′N, 111°7′E) and Hougou (34°50′N, 111°8′E) subsections which are ~1 km away from each other. In the field, the two subsections can be correlated by the marker layers of L9 and S9 (Figs. 3a, b). Our section is ~15 km to the east of the Huangdigou section (Wang et al., 1999), and ~2 km to the north of the modern Yellow River (Fig. 2a).

The strata in the Zhangcun section are horizontal, with a thickness over 210 m. According to our field observations, the pale yellow huge-thick lenticular sandstones and interbed green-grayish calcareous mudstones with horizontal bedding below the 193 m of the section (Fig. 3d) were the upper part of the Youhe Formation; the interbed pale yellow siltstones and green-grayish calcareous mudstones with horizontal bedding between 172.7 and 193 m (Figs. 3c, d) were the lower part of the Sanmen Formation; and the water-reworked loess between 172.7 and 122.5 m were the upper part of the Sanmen Formation (Fig. 3c). The loess-paleosol sequences between 122.5 and 10 m can be identified as S22 to S4 (Figs. 3a, b) in the field based on the marker layers of S5, S8, L9, S9, and L15 (Liu, 1985). No hiatus was found in this section during our field survey.

3.2. Samples and measurements

In this study, 1830 samples at 10-cm stratigraphic intervals were collected from the Zhangcun section for magnetic susceptibility analysis, 237 oriented block samples were collected with sample spacing of 0.5–1.5 m for paleomagnetic investigation, and 6 representative samples (17.7m, 24 m, 120.5 m, 123 m, 164.5 m, and 188.7 m) were collected from the different sedimentary facies for rock magnetism analyses.

The paleomagnetic and rock magnetic measurements were performed at the

Environmental Magnetism Laboratory of China University of Geosciences, Wuhan. Prior to demagnetization, we measured the low-field magnetic susceptibility of all the 1830 samples, and temperature-dependence of magnetic susceptibility (χ-T curves), isothermal remanent magnetization (IRM) acquisition, and first-order reversal curves (FORC) for the 6 representative samples. The χ-T curves were measured in an argon atmosphere at a frequency of 976 Hz from room temperature (25 °C) up to 700 °C and back to room temperature using a KLY-3S Kappabridge equipped with a CS-3 high-temperature controlling system. The IRM acquisition curves and FORC diagrams were measured using a MicroMag 2900 alternating gradient magnetometer (Princeton Measurements Corp., USA).

In the laboratory, 2 cm cubic specimens were cut from each oriented block sample for thermal demagnetization. All specimens were subjected to progressively thermal demagnetization in a TD-48SC thermal demagnetizer which has a residual field <10 nT. Thermal demagnetization up to 680 °C included a maximum of 17 steps with intervals of 50 °C below 500 °C and 20–30 °C above. Remanence measurements were made using a 2G-755-4k cryogenic magnetometer housed in a magnetically shielded room (background field <200 nT). The results are available from the Supplementary data.

4. Results

4.1. Rock magnetic results

χ-T curve has been used routinely to identify changes in mineralogy of natural samples during thermal treatment and thus reveal the magnetic mineralogy (Deng et al., 2004, 2006; Ao et al., 2010). During heating, χ of all samples shows a decrease trend between ~300°C and 400°C and a more pronounced drop between 400 and 580°C (Fig. 4). The former drop indicates the inversion from strongly magnetic but thermally unstable maghemite to weakly hematite (Deng et al., 2004, 2006), and the latter one indicates that magnetite is the major contributor to the susceptibility (Deng et al., 2004, 2006). There are also several differences among different type of samples in their χ-T curves. For the paleosol samples, the susceptibility shows a steady increase trend below ~250°C during the heating process (Figs. 4a, c, e), suggesting the gradual unblocking of fine-grained ferrimagnetic particles (Deng et al., 2004, 2006). In contrast, the loess samples lack such an increase trend in susceptibility (Figs. 4b, d), indicating that they contain less fine-grained pedogenic maghemite grains. Further, the loess samples also show significantly different patterns of magnetic susceptibility changes from paleosol samples during thermal treatment, and the magnetic susceptibility of loess samples during cooling was significantly higher than during heating. The increase in susceptibility has been attributed to the transformation from iron-containing silicates/clays to magnetite during thermal treatment (Deng et al., 2004, 2006; Ao et al., 2009). However, the lacustrine sample lack such an increase in susceptibility during cooling (Fig. 4f), which indicates that such transformation is not significant.

[Figure 4]

Figure 5 shows IRM curves for representative samples from the Zhangcun section. All IRM acquisition curves exhibit a major increase below 0.3 T, implying that the magnetic minerals are dominated by magnetically soft components with low coercivity, such as magnetite and maghemite. However, the paleosol samples (Figs. 5a, c, e) display a more rapidly rise trend below 100 mT than the loess samples (Figs. 5b, d), indicating that the paleosol samples contain higher concentrations of magnetite and maghemite. These characteristics are consistent with the χ-T results (Fig. 4), as well as the results from other loess sections in the Chinese Loess Plateau (e.g., Deng et al., 2004, 2006; Wang et al., 2005). The curve of lacustrine sample shows relatively higher SIRM (Fig. 5f) than that of loess and paleosol samples, indicating that it contains relatively higher content of high-coercivity hematite.

[Figure 5]

The FORC diagrams can provide information about variations in magnetic mineralogy and grain size, as well as particle switching fields and local interaction fields for the assemblage of magnetic particles within a sample (Roberts et al., 2014; Hu et al., 2015). The FORC diagrams (Fig. 6) show that all samples from the Zhangcun section have a low coercivity (<100 mT), consistent with a magnetic mineralogy dominated by magnetite and maghemite as suggested by the χ-T and IRM acquisition curves (Figs. 4, 5). The paleosol samples (Figs. 6a, c, e) are characterized by one or two closed inner contours and outer contours that diverge along the Bu axis (Bu represents the interaction field among magnetic grains), which indicates the presence of single-domain and pseudo-single-domain magnetites in these samples (Roberts et al., 2014). In contrast to the paleosol samples, the loess and lacustrine samples contain no/less closed contours with larger vertical spread (Figs. 6b, d, f), indicating a dominance of multidomain magnetite in these samples (Roberts et al., 2014). Overall, the magnetic minerals in the Zhangcun section were dominant by multidomain and pseudo-single-domain magnetite, consistent with previous FORC studies from the Chinese Loess Plateau (Hu et al., 2015).

[Figure 6]

4.2. Characteristic remanent magnetization and magnetic susceptibility results

Demagnetization results were evaluated on stereographic projections and vector end point orthogonal diagrams (Fig. 7a–f). For most samples, after removing a viscous magnetization component below 250°C, a Characteristic Remanent Magnetization (ChRM) component was successfully isolated between 300 and 550°C. This suggests that magnetite is the main carrier of ChRM, which is further supported by the rock magnetism analyses above (Figs. 4–6). For some samples from the Sanmen Formation (Fig. 7e–f), the ChRM component was isolated between 300 and 620 °C (up to 650 °C), which suggests that the carrier of ChRM is a combination of magnetite and hematite (Figs. 5f, 6f). The ChRM directions were calculated on a minimum of four consecutive steps (Kirschvink, 1980), with maximum angular deviation (MAD) above 15° being rejected from further analyses. A total of 22.4% samples, most from loess layers L9 and L15, showed unstable demagnetization trajectories such that ChRM directions could not be isolated. The remaining 184 samples with reliable ChRM directions (77.6%) are used to calculate the virtual geomagnetic pole (VGP) latitudes and define the geomagnetic polarity zones.

[Figure 7]

Stratigraphically, the magnetic susceptibility of the Zhangcun section exhibits two abrupt and significant upward-increase trends at the depth of 172.7 and 122.5 m (Fig. 8a). Specifically, the lower part of Sanmen Formation (193–172.7 m) exhibits the lowest magnetic susceptibility value (24 SI on average) and fluctuations, and the magnetic susceptibility value is doubled (54.5 SI on average) in the upper part of Sanmen Formation (172.7–122.5 m), with the highest value occurring in the paleosol layer S26. The magnetic susceptibility value and fluctuations further increased in the loess-paleosol sequences (above 122.5 m), with an average value of 79.2 SI between S22 and S9.

5. Discussion

5.1. Age constraints on the upper Pliocene-Pleistocene sediments in the Sanmenxia sub-basin

Based on the above 184 reliable paleomagnetic samples, five normal polarity zones

(N1 to N5, Fig. 8a) are identified in the Zhangcun section. According to the previous magnetostratigraphic investigations on the Chinese loess (e.g., Liu, 1985; Wang et al., 2005; Zheng et al., 2007; Liu et al., 2015; Deng et al., 2019), we can readily correlate the polarity zones from the Zhangcun section with the GPTS 2012 (Ogg, 2012). Obviously, the normal polarity zone N1 (10–53.3 m) above L8 should be correlated to C1n (Brunhes), and the normal polarity zones N3 (S11–S13) and N4 (including S25–S26) should be correlated to C1r.1n (Jaramillo) and C2n (Olduvai), respectively (Fig. 8a). This correlation is consistent with the Caocun section (Zhao et al., 2000; Wang et al., 2005) that is ~18 km southwest to the Zhangcun section (Fig. 8b), as well as other classical loess sections, such as Luochuan, Xifeng, and Weinan sections (Liu, 1985; Liu et al., 2010, 2015). Based on the above correlation, we can further correlate the polarity transition at 188.5 m in the Zhangcun section to the Matuyama/Gauss boundary (Fig. 8a). Our magnetostratigraphic results on loess-paleosol sequences and the Sanmen Formation are consistent with previous studies (e.g., Liu, 1985; Yue, 1996; Han et al., 1997; Zhao et al., 2000; Wang et al., 2005; Zheng et al., 2007; Liu et al., 2010, 2015; Deng et al., 2019). For the 10 m-thick normal polarity zone N2 in the loess layer L9 (Fig. 8a), it cannot be correlated to the GPTS 2012 (Ogg, 2012). This anomalous normal polarity zone was also reported in other loess sections across the Chinese Loess Plateau, such as the Caocun (Fig. 8b) (Wang et al., 2005), Mangshan (Zheng et al., 2007), and Luochuan sections (Liu et al., 2010), which was interpreted as the product of remagnetization (Wang et al., 2005; Pan et al., 2021).

[Figure 8]

According to the above correlation (Fig. 8a), the boundary age between Youhe and Sanmen Formations in the Sanmenxia Subbasin was ~2.7 Ma, which was very close to that age (~2.6 Ma) in the Weihe Subbasin (Yue, 1996; Han et al., 1997; Liu and Xue, 2004). In addition, the top age (~1.6 Ma) of the Sanmen Formation at the Zhangcun section was also broadly consistent with other sections in the Fenwei Basin. For example, in the Weihe Subbasin, the top age of the Sanmen Formation at the Wujiabao (Sun et al., 1988), W7 core (Ge et al., 1991), Shijiawan (Han et al., 1997), and Songjiabeigou (Yue, 1996) were ~1.8 Ma, 1.67 Ma, 1.9 Ma, and 1.2 Ma, respectively (see Fig. 2a for locations); In the Yuncheng Subbasin, the top age of the Sanmen Formation at the P5 core, P4 core, Linyi, and Yangfan sections from the northern, middle, and eastern part of the basin were ~1.9, ~1.7, and 1.2 Ma (Wang et al., 2002a; Li et al., 2004; Qiu et al., 2018), respectively (see Fig. 2a for locations).

The aforementioned studies suggested that the end of the Sanmen Formation was between 1.9 and 1.2 Ma, albeit there were slight differences among different sites. This is significantly different from the results obtained from the magnetostratigraphic investigation at the Huangdigou section from the Sanmenxia Subbasin which suggested that the top age of the Sanmen Formation was at ~0.15 Ma and therefore the integration of the Yellow River was also at ~0.15 Ma (Wang et al., 1999). As shown in Figure 9, our re-interpretation of the magnetostratigraphic results of Wang et al. (1999) suggests an improper correlation between the polarity zones and the GPTS in their study, due to a hiatus in their section between ~2.6 and 0.15 Ma. Our re-interpretation is further supported by the four observations explained below.

[Figure 9]

Firstly, according to our field investigation and the description of Wang et al. (1999) and Jiang et al. (2007), the huge-thick sandstones intercalated with green-grayish calcareous mudstones on the upper part of the Huangdigou section indeed belong to the upper Pliocene Youhe Formation rather than the Middle and Upper Pleistocene strata. This is further supported by the re-interpretation (Fig. 9b), which is also consistent with the age of the Youhe Formation (Yue, 1996; Han et al., 1997; Liu and Xue, 2004). Secondly, the strata reported by Wang et al. (1999) and Jiang et al. (2007) did not include the Sanmen Formation and the above loess-paleosol sequences (S22–L2) (Figs. 8 and 9), albeit these strata were widely exposed along the Yellow River valley in the Sanmenxia Subbasin, such as the Xihoudu (Kong et al., 2013) and Dongpogou (He et al., 1984) sections (see Fig. 2a for locations), the Miaoxia and Yangwa (~1 km away from the Huangdigou section) sections (Wang et al., 2000), and the Bangou section (~4 km away from the Huangdigou section, Fig. 3e). The Sanmen Formation and the above loess-paleosol sequences can be also correlated to other subbasins within the Fenwei Basin, such as Weihe (Yue, 1996; Han et al., 1997; Liu and Xue, 2004) and Yuncheng (Wang et al., 2002a; Li et al., 2004) Subbasins. Thirdly, according to our field investigation, the Sanmen Formation and above loess-paleosol sequences (S22–L2) at the Huangdigou section were eroded by the Yellow River. At least five Yellow River terraces have been found near the Huangdigou section with an age of ~1.24 Ma (T5), ~0.86 Ma (T4), ~0.62 Ma (T3), ~0.129 Ma (T2), and ~0.012 Ma (T1), respectively (Kong et al., 2014; Hu et al., 2017; Li et al., 2017), and all these terraces were covered by loess-paleosol sequences. As the top of the Huangdigou section is covered by S1 and L1 (Wang et al., 1999; Jiang et al., 2007), it indeed corresponds to the T2 terrace (~0.129 Ma) of the Yellow River (Hu et al., 2017), suggesting that the Huangdigou section contains a hiatus between the Youhe Formation and the paleosol S1. According to our re-interpretation of the magnetostratigraphic results of Wang et al. (1999), this hiatus is between ~2.6 and 0.15 Ma (Fig. 9b). Finally, the biostratigrahic investigation from the Huangdigou section suggested that this section may include only the strata from the upper Miocene to the lower Pleistocene, but not the Middle Pleistocene (Yuan, 1986). All these observations show that the Huangdigou section lacks of the Sanmen Formation and the above loess-paleosol sequences (S22–L2) so that it could not record the dry up of the Sanmen paleolake and thus the suggestion of the integration of the Yellow River at ~0.15 Ma is questionable.

5.2. Magnetic susceptibility and sedimentary records and their implications for the integration of the Yellow River

The magnetic susceptibility records in the Zhangcun section exhibits two abrupt increases at ~2.4 and ~1.6 Ma, which are consistent with the changes of sedimentary facies at the depth of 172.7 m and 122.5 m, respectively (Fig. 8a). However, it is noteworthy that there is no counterpart increase of magnetic susceptibility in the typical Quaternary loess-paleosol sequences at the nearby Caocun section (Zhao et al., 2000; Wang et al., 2005), albeit their magnetic susceptibility curves between S22 and S4 can be well correlated to each other (Fig. 8). This suggests that the two increases of magnetic susceptibility in the Zhangcun section were due to changes in sedimentary facies rather than regional climate. Specifically, the increase of magnetic susceptibility at ~2.4 Ma responded to the transition from the lake environment to an alternation of shallow lake and floodplain condition, indicating change from a reducing environment to oxidizing one. This sedimentary change would reduce the dissolution of magnetic minerals and thus increase the value of magnetic susceptibility (Ao et al., 2010). The increase in value and fluctuations of magnetic susceptibility at the depth of 122.5 m (~1.6 Ma) responded to an irreversible dried up of the Sanmen paleolake and the onset accumulation of typical loess-paleosol sequences. A significant change in sedimentary facies is also found at this depth. The pale-yellow calcareous siltstone layers below this depth are mostly laminated and without pedological features, which are significantly different from the loess and paleosol units above; in the paleosol layers below this depth, the pedogenesis is very weak, which is probably due to the influence of drainage and soil humidity. Consequently, the weathering degree and the redness of the sediments below this depth are overall weaker than the loess-paleosol sequences above. In addition, the laminated deposits and conglomerate lenses disappear above this depth (Fig. 8). These sedimentary changes have resulted in a normal pedogenic condition and increased the values and fluctuations of magnetic susceptibility since 1.6 Ma, leading to a clear manifestation of the glacial-interglacial variations of the Eastern Asian summer monsoon (An et al., 1991; Zhao et al., 2000; Deng et al., 2006).

The dry up of the Sanmen paleolake could be attributed to two possible factors. The first one was the gradually aridification of the regional climate (Han et al., 1997; Deng et al., 2006) associated with the global cooling since the latest Pliocene (Lisiecki and Raymo, 2005), and the second one was the capture of the Fenwei Basin by the Yellow River. The upward shallowing of the Sanmen paleolake between 2.7 and 1.6 Ma was probably due to the long-term cooling and aridification in regional climate. However, the absent of widespread evaporites in the Fenwei Basin suggests that the irreversible dried up of the Sanmen paleolake at ~1.6 Ma was not due to regional climate, because the dry up of the endorheic mega-lake would form widespread evaporites (Warren, 2010), such as the salar of Uyuni in the central Bolivian Altiplano (Risacher and Fritz, 2000) and the Qarhan salty lake in the Qaidam Basin (Chen and Bowler, 1986). Further, the magnetic susceptibility records from the Caocun section suggested that there was no significant aridification in regional climate at ~1.6 Ma (Fig. 8b). Therefore, the irreversible dried up of the Sanmen paleolake at ~1.6 Ma was most likely linked to the capture of the Fenwei Basin that associated with the integration of the Yellow River. It is noteworthy that some sections from the Weihe and Yuncheng Subbasins shown the occurrence of loess-paleosol sequences were ~0.2–0.3 Ma earlier (e.g., Sun et al., 1988; Han et al., 1997; Wang et al., 2002a) or later (e.g., Yue, 1996; Li et al., 2004; Qiu et al., 2018) than 1.6 Ma, which may be due to these sections are located in the central or on the edge of these subbasins. This is supported by the phenomenon that the Shijiawan and Wujiabao sections on the edge of the Weihe Subbasin shown an early termination of the lacustrine facies (Sun et al., 1988; Han et al., 1997). As our section is very close to the outlet of the Sanmen paleolake, and the altitude of the youngest lacustrine deposition in this section is ~300 m higher than the North China Plain, it would be very sensitive to the rapid fall of the lake level when the Sanmenxia Subbasin was captured by the Yellow River.

Based on the conglomerates underlying the late Pliocene Hipparion Red-Earth Formation in the region of the Sanmen Gorge, some researchers suggested that a Pliocene Yellow River flowed through the Sanmen Gorge (e.g., Li and Yang, 1991). However, recent studies (Hu et al., 2017; Xiong et al., 2017, 2018) and our field investigation have demonstrated that these conglomerates were the products of ancient alluvial fan deposits accumulated on the Tangxian planation surface. This is supported by three lines of observations. 1) The Pliocene conglomerates were widespread on the Tangxian planation surface in the piedmont of the Xiaoshan and Zhongtiaoshan Mountains (Hu et al., 2017; Xiong et al., 2017, 2018), but not only distributed in the region of Sanmen Gorge. 2) These conglomerates are mostly subangular and subrounded, poorly sorted according to our field investigation. In contrast, the conglomerates of the Yellow River terraces are mostly rounded and subrounded, well sorted, suggesting that the Pliocene conglomerates were not the deposits of the Yellow River. And 3) our recent detrital-zircon provenance studies from three boreholes in the lower Yellow River floodplain demonstrated that the onset of input of materials from the Middle and/or Upper Reaches into the Lower Reaches occurred at ~1.6 Ma (Xiao et al., 2020), precluding a Pliocene Yellow River flowing through the Sanmen Gorge.

Some previous studies suggested a late Miocene or Pliocene age of the Yellow River based on the ages of conglomerate layers along the Jinshan Gorge (e.g., Wang, 1925; Liu, 2017, 2020). However, some researchers augured that these conglomerate layers in the Hipparion Red-Earth Formation were the alluvial fan deposits which reflect the uplift and denudation of the Lvliang Mountains, but not the terrace deposits of the ancient Yellow River (Li et al., 2009; Xu et al., 2019). Xiao et al. (2020) proposed a conceptual model that could reconcile different views on the timing of integration of the Yellow River based on the fact that no sediments from the Middle and/or Upper Reaches could be transported into the Lower Reaches until ~1.6 Ma (Yao et al., 2017; Zhang et al., 2019; Xiao et al., 2020). This model suggests that these >1.6 Ma conglomerates/fluvial terraces along the Jinshan Gorge would belong to an ancient endorheic drainage network emptied into the mega Fenwei Basin. In this sense, the >1.6 Ma conglomerates/fluvial terraces in the Middle and Upper Reaches (e.g., Nie et al., 2015; Guo et al., 2018) could not belong to the integrated Yellow River.

Regarding the mechanism for the capture of the Sanmen paleolake, some previous studies suggested that it was caused by lake spillover (Kong et al., 2014; Hu et al., 2017) or local/regional tectonisms (e.g., Wu et al., 1998; Wang et al., 2002b). However, our sedimentary records suggested a gradually shallowing trend of the lake level since the latest Pliocene, which was consistent with the global and regional climate changes (Han et al., 1997; Zhao et al., 2000; Lisiecki and Raymo, 2005; Deng et al., 2006). For the local/regional tectonisms, it is shown that they were much earlier than 1.6 Ma (Xiao et al., 2020), thus not likely the main factors for the capture of the Sanmen paleolake. Xiao et al. (2020) proposed that the onset of large-amplitude and high-frequency sea level changes associated with increasing climate instability since late Pliocene may have accelerated fluvial headwater erosion and finally cut through the ~100 km-wide Xiaoshan Mountain and subsequently integrated the whole Yellow River system in the early Pleistocene.

6. Conclusions

This study provides a detailed magnetostratigraphic and magnetic susceptibility study of a lacustrine-loess section from the Sanmenxia Subbasin and indicates that the Sanmen paleolake was captured by the Yellow River at ~1.6 Ma, supporting our previous detrital-zircon provenance studies from three boreholes in the lower Yellow River floodplain. Our results challenge the chronostratigraphic framework for the Sanmen Formation from the Huangdigou section in the Sanmenxia Subbasin, and precluded the idea that the timing of the integration of the Yellow River was at ~0.15 Ma. Our sedimentary records suggested a gradually shallowing trend of the lake level since the latest Pliocene, implying that the integration of the Yellow River was by upstream capture rather than lake spillover.

Declaration of competing interest

The authors declare that they have no known competing financial interests or personal relationships that could have appeared to influence the work reported in this paper.

Acknowledgments

We are grateful to two anonymous reviewers for their thorough and valuable comments on an early version. This study is supported by the National Science Foundation of China (Grant nos. 41888101, 41830319) and the “Strategic Priority Research Program” of the Chinese Academy of Sciences (Grants: XDB26000000). We are grateful to Drs. Huiru Xu, Yingchao Xu, Canfa Wang, and Shijin Zhao for field and laboratory assistance.

Appendix A. Supplementary data

Supplementary data to this article can be found online at https://XXX.

References

An, Z.S., Kukla, G., Porter, S.C., Xiao, J.L., 1991. Magnetic susceptibility evidence of monsoon variation on the Loess Plateau of central China during the last 130,000 years. Quat. Res. 36, 29–36. https://doi.org/10.1016/0033-5894(91)90015-W.

Andersson, J.G., 1923. Essays on the Cenozoic of Northern China. Memoir of the Geological Survey of China (Ser. A), 152 pp.

Ao, H., Dekkers, M.J., Deng, C., Zhu, R., 2009. Palaeclimatic significance of the Xiantai fluvio-lacustrine sequence in the Nihewan Basin (North China), based on rock magnetic properties and clay mineralogy. Geophys. J. Int. 177, 913–924. doi: 10.1111/j.1365-246X.2008.04082.x

Ao, H., Deng, C.L., Dekkers, M.J., Liu, Q.S., 2010. Magnetic mineral dissolution in Pleistocene fluvio-lacustrine sediments, Nihewan Basin (North China). Earth Planet. Sci. Lett. 292, 191–200. https://doi.org/10.1016/j.epsl.2010.01.035.

Bridgland, D.R., Westaway, R., Hu, Z.B., 2020. Basin inversion: A worldwide Late Cenozoic phenomenon. Glob. Planet. Change. 193, 103260. https://doi.org/10.1016/j.gloplacha.2020.103260.

Chen, K.Z., Bowler, J.M., 1986. Late pleistocene evolution of salt lakes in the Qaidam basin, Qinghai province, China. Palaeogeogr. Palaeoclimatol. Palaeoecol. 54, 87–104. https://doi.org/10.1016/0031-0182(86)90119-7.

Craddock, W.H., Kirby, E., Harkins, N., Zhang, H.P., Shi, X.H., Liu, J.H., 2010. Rapid fluvial incision along the Yellow River during headward basin integration. Nat. Geosci. 3, 209–213. https://doi.org/10.1038/ngeo777.

Deng, C.L., Shaw, J., Liu, Q.S., Pan, Y.X., Zhu, R.X., 2006. Mineral magnetic variation of the Jingbian loess/paleosol sequence in the northern Loess Plateau of China: Implications for Quaternary development of Asian aridification and cooling. Earth Planet. Sci. Lett. 241, 248–259. https://doi.org/10.1016/j.epsl.2005.10.020.

Deng, C.L., Zhu, R.X., Verosub, K.L., Singer, M.J., Vidic, N.J., 2004. Mineral magnetic properties of loess/paleosol couplets of the central loess plateau of China over the last 1.2 Myr. J. Geophys. Res. 109, B01103. https://doi.org/10.1029/2003jb002532.

Deng, C.L., Hao, Q.Z., Guo, Z.T., Zhu, R.X., 2019. Quaternary integrative stratigraphy and timescale of China. Sci. China Earth Sci. 62, 324–348. https://doi.org/10.1007/s11430-017-9195-4.

Deng, Q.D., Zhang, P.Z., Ran, Y.K., Yang, X.P., Min, W., Chu, Q.Z., 2003. Basic characteristics of active tectonics of China. Sci. China (Ser. D) 46, 356–372. https://doi.org/10.1360/03yd9032.

Fang, X.M., Garzione, C., Van der Voo, R., Li, J.J., Fan, M.J., 2003. Flexural subsidence by 29 Ma on the NE edge of Tibet from the magnetostratigraphy of Linxia Basin, China. Earth Planet. Sci. Lett. 210, 545–560. https://doi.org/10.1016/S0012-821X(03)00142-0.

Fang, X.M., Yan, M.D., Van der Voo, R., Rea, D.K., Song, C.H., Parés, J.M., Gao, J.P., Nie, J.S., Dai, S., 2005. Late Cenozoic deformation and uplift of the NE Tibetan Plateau: Evidence from high-resolution magnetostratigraphy of the Guide Basin, Qinghai Province, China. Geol. Soc. Am. Bull. 117, 1208–1225. https://doi.org/10.1130/B25727.1.

Ge, T.M., Fan, L.M., Xu, X., Li, S.Z., Zheng, H.R., 1991. Magnetostratigraphic study for borehole W7 from Yancun, Weinan. Mar. Geol. & Quat. Geol. 11, 59–71 (in Chinese with English abstract).

Guo, B., Liu, S., Peng, T., Ma, Z., Feng, Z., Li, M., Li, X., Li, J., Song, C., Zhao, Z., Pan, B., Stockli, D.F., Nie, J., 2018. Late Pliocene establishment of exorheic drainage in the northeastern Tibetan Plateau as evidenced by the Wuquan Formation in the Lanzhou Basin. Geomorphology 303, 271–283. https://doi.org/10.1016/j.geomorph.2017.12.009.

Han, H.Y., Zhang, Y., Yuan, Z.X., 2002. The evolution of Weihe Down-faulted Basin and the movement of the fault blocks. J. Seismol. Res. 25, 362–368 (in Chinese with English abstract). https://doi.org/10.3969/j.issn.1000-0666.2002.04.010.

Han, J., Fyfe, W.S., Longstaffe, F.J., Palmer, H.C., Yan, F.H., Mai, X.S., 1997. Pliocene-Pleistocene climatic change recorded in fluviolacustrine sediments in central China. Palaeogeogr. Palaeoclimatol. Palaeoecol. 135, 27–39. https://doi.org/10.1016/S0031-0182(97)00019-9.

He, P.Y., Liu, L.S., Yu, Q.Y., 1984. The age of the “Sanmen Series” and the evolution of its depositional environment discussed in the light of the Dongpogou section in the Sanmen Gorge area. Geol. Rev. 30, 161–169 (in Chinese with English abstract).

Hu, P.X., Liu, Q.S., Heslop, D., Roberts, A.P., Jin, C.S., 2015. Soil moisture balance and magnetic enhancement in loess-paleosol sequences from the Tibetan Plateau and Chinese Loess Plateau. Earth Planet. Sci. Lett. 409, 120–132. https://doi.org/10.1016/j.epsl.2014.10.035.

Hu, X.M., Li, Y.L., Yang, J.C., 2005. Quaternary paleolake development in the Fen River basin, North China. Geomorphology 65, 1–13. https://doi.org/10.1016/j.geomorph.2004.06.008.

Hu, Z.B., Pan, B.T., Bridgland, D., Vandenberghe, J., Guo, L.Y., Fan, Y.L., Westaway, R., 2017. The linking of the upper-middle and lower reaches of the Yellow River as a result of fluvial entrenchment. Quat. Sci. Rev. 166, 324–338. https://doi.org/10.1016/j.quascirev.2017.02.026.

Jiang, F.C., Fu, J.L., Wang, S.B., Sun, D.H., Zhao, Z.Z., 2007. Formation of the Yellow River, inferred from loess-palaeosol sequence in Mangshan and lacustrine sediments in Sanmen Gorge, China. Quat. Int. 175, 62–70. https://doi.org/10.1016/j.quaint.2007.03.022.

Kaakinen, A., Lunkka, J.P., 2003. Sedimentation of the Late Miocene Bahe Formation and its implications for stable environments adjacent to Qinling mountains in Shaanxi, China. J. Asian Earth Sci. 22, 67–78. https://doi.org/10.1016/S1367-9120(03)00044-0.

Kirschvink, J.L., 1980. The least-squares line and plane and the analysis of palaeomagnetic data. Geophys. J. R. Astron. Soc. 62, 699–718. https://doi.org/10.1111/j.1365-246X.1980.tb02601.x.

Kong, P., Jia, J., Zheng, Y., 2013. Cosmogenic ^{26}Al/^{10}Be burial dating of the Paleolithic at Xihoudu, North China. J. Hum. Evol. 64, 466–470. https://doi.org/10.1016/j.jhevol.2013.01.016.

Kong, P., Jia, J., Zheng, Y., 2014. Time constraints for the Yellow River traversing the Sanmen Gorge. Geochem.

Geophys. Geosyst. 15, 395–407. https://doi.org/10.1002/2013GC004912.

Li, J., Yue, L., Xu, Y., Sun, L., Sun, B., Wang, X., Bai, B., 2009. Uplift of Lvliang Mountains and evolution of Huanghe River—Evidence from gravel beds in piedmont. Sci. Geogr. Sin. 29, 582–586 (in Chinese with English abstract). http://geoscien.neigae.ac.cn/CN/Y2009/V19/I4/582.

Li, R., Yang, M., 1991. Relationship between developments of the Huanghe and Yongding rivers and the evolution of the fossil lakes of the Cenozoic era in the drainage area. Chin. Geogr. Sci. 1, 234–247. http://egeoscien.neigae.ac.cn/EN/Y1991/V1/I3/234.

Li, Y.L., Shi, X.M., Fu, J.L., Yang, J.C., 2004. Geomorphic transformational event around 1.2 Ma B.P. in the southern Shanxi Province. Sci. Geogr. Sin. 24, 292–297 (in Chinese with English abstract). https://doi.org/10.3969/j.issn.1000-0690.2004.03.007.

Li, X., Ao, H., Dekkers, M.J., Roberts, A.P., Zhang, P., Lin, S., Huang, W., Hou, Y., Zhang, W., An, Z., 2017. Early Pleistocene occurrence of Acheulian technology in North China. Quat. Sci. Rev. 156, 12–22. http://dx.doi.org/10.1016/j.quascirev.2017.02.026.

Lisiecki, L.E., Raymo, M.E., 2005. A Pliocene-Pleistocene stack of 57 globally distributed benthic $\delta^{18}O$ records. Paleoceanography 20, PA1003, https://doi.org/doi:1010.1029/2004PA001071.

Liu, H.J., Xue, X.X., 2004. Discussion on the Cenozoic and its chronology in the Weihe River basin. J. Earth Sci. & Environ. 26, 1–5 (in Chinese with English abstract). https://doi.org/10.3969/j.issn.1672-6561.2004.04.001.

Liu, H.J., Xue, X.X., Li, Y.X., 2006. Calculation on the paleosalinity of the ancient Sanmen Lake in the Weinan Area of Weihe River Basin. J. Northwest Univ. (Nat. Sci. Ed.). 36, 112–114 (in Chinese with English abstract). https://doi.org/10.3321/j.issn:1000-274X.2006.01.027.

Liu, J.H., Zhang, P.Z., Lease, R.O., Zheng, D.W., Wan, J.L., Wang, W.T., Zhang, H.P., 2013. Eocene onset and late Miocene acceleration of Cenozoic intracontinental extension in the North Qinling range-Weihe graben: Insights from apatite fission track thermochronology. Tectonophysics 584, 281–296. https://doi.org/10.1016/j.tecto.2012.01.025.

Liu, Q.S., Jin, C.S., Hu, P.X., Jiang, Z.X., Ge, K.P., Roberts, A.P., 2015. Magnetostratigraphy of Chinese loess-paleosol sequences. Earth-Sci. Rev. 150, 139–167. https://doi.org/10.1016/j.earscirev.2015.07.009.

Liu, T.S., 1985. Loess and the Environment. Science Press, Beijing, 481 pp.

Liu, W.M., Zhang, L.Y., Sun, J.M., 2010. High resolution magnetostratigraphy of the Luochuan loess-paleosol sequence in the central Chinese Loess Plateau. Chin. J. Geophys. 53, 888–894 (in Chinese with English abstract). https://doi.org/10.3969/j.issn.0001-5733.2010.04.013.

Liu, Y., 2017. Magnetostratigraphy and origin of Neogene conglomerate in the Hequ, Shanxi Province. Quat. Sci. 37, 597–611 (in Chinese with English abstract). http://www.dsjyj.com.cn/CN/Y2017/V37/I3/597.

Liu, Y., 2020. Neogene fluvial sediments in the northern Jinshaan Gorge, China: Implications for early development of the Yellow River since 8 Ma and its response to rapid subsidence of the Weihe-Shanxi Graben. Palaeogeogr. Palaeoclimatol. Palaeoecol. 546, 109675. https://doi.org/10.1016/j.palaeo.2020.109675.

Nie, J., Stevens, T., Rittner, M., Stockli, D., Garzanti, E., Limonta, M., Bird, A., Andò, S., Vermeesch, P., Saylor, J., Lu, H., Breecker, D., Hu, X., Liu, S., Resentini, A., Vezzoli, G., Peng, W., Carter, A., Ji, S., Pan, B., 2015. Loess Plateau storage of Northeastern Tibetan Plateau-derived Yellow River sediment. Nat. Commun. 6, 8511. http://dx.doi.org/10.1038/ncomms9511.

Ogg, J.G., 2012. Geomagnetic polarity time scale, in: Gradstein, F.M., Ogg, J.G., Schmitz, M.D., Ogg, G.M. (Eds.), The Geologic Time Scale 2012. Elsevier, Amsterdam, pp. 85–114. https://doi.org/10.1016/B978-0-444-59425-9.00005-6.

Pan, Q., Xiao, G., Zhao, Q., Chen, R., Ao, H., Shen, Y., Cheng, J., Zhu, Z., 2021. The Jaramillo subchron in Chinese loess-paleosol sequences. Palaeogeogr. Palaeoclimatol. Palaeoecol. 572, 110423. https://doi.org/10.1016/j.palaeo.2021.110423.

Qiu, Y., Ao, H., Zhang, Y., Shu, P., Li, Y., Li, X., Zhang, P., 2018. Magnetostratigraphic dating of the Linyi Fauna and implications for sequencing the mammalian faunas on the Chinese Loess Plateau. Quat. Res. 89, 629–644. https://doi.org/10.1017/qua.2017.83.

Risacher, F., Fritz, B., 2000. Bromine geochemistry of salar de Uyuni and deeper salt crusts, Central Altiplano, Bolivia. Chem. Geol. 167, 373–392. https://doi.org/10.1016/S0009-2541(99)00251-X.

Rits, D.S., Prins, M.A., Troelstra, S.R., van Balen, R.T., Zheng, Y., Beets, C.J., Wang, B., Li, X.Q., Zhou, J., Zheng, H.B., 2016. Facies analysis of the Middle and Late Quaternary sediment infill of the northern Weihe Basin, Central China. J. Quat. Sci. 31, 152–165. https://doi.org/10.1002/jqs.2853.

Roberts, A.P., Heslop, D., Zhao, X., Pike, C.R., 2014. Understanding fine magnetic particle systems through use of first-order reversal curve diagrams. Rev. Geophys. 52, 557–602. https://doi.org/10.1002/2014RG000462.

Shi, W., Chen, L., Chen, X.Q., Cen, M., Zhang, Y., 2019. The Cenozoic tectonic evolution of the faulted basins in the northern margin of the Eastern Qinling Mountains, Central China: Constraints from fault kinematic analysis. J. Asian Earth Sci. 173, 204–224. https://doi.org/10.1016/j.jseaes.2019.01.018.

Sun, J.Z., Zhao, J.B., Wei, M.J., Ge, T.M., Wen, S.Y., Fan, L.M., Geng, H.P., 1988. New paleomagnetic data of the Wujiabao section. Hydro. & Eng. Geol. 5, 44–48 (in Chinese with English abstract).

Tan, C.X., Sun, W.F., Zhang, C.S., Wu, S.R., Shi, J.S., Li, B., Wang, T., 2011. Engineering geological features from borehole cores for typical loess section in Baoji region of Loess Plateau. J. Eng. Geol. 19, 732–748 (in Chinese with English abstract). https://doi.org/10.3969/j.issn.1004-9665.2011.05.014.

Wang, B., Zheng, H.B., He, Z., Wang, P., Kaakinen, A., Zhou, X.Y., 2014. Middle Miocene eolian sediments on the southern Chinese Loess Plateau dated by magnetostratigraphy. Palaeogeogr. Palaeoclimatol. Palaeoecol. 411, 257–266. https://doi.org/10.1016/j.palaeo.2014.07.007.

Wang, C.C., 1925. The physiographioal history of the Yellow River between Shansi and Shensi. Bull. Geol. Soc. China 4, 87–91. https://doi.org/10.1111/j.1755-6724.1925.mp4002002.x.

Wang, P.X., Wang, N.W., Bao, J.S., 1982. Discovery of the Cenozoic foraminifera in the Fen-wei Basin and its significance. Geol. Rev. 28, 93–100 (in Chinese with English abstract). https://doi.org/10.3321/j.issn:0371-5736.1982.02.001.

Wang, Q., Li, C.G., Tian, G.Q., Zhang, W.Z., Liu, C., Ning, L.Y., Yue, J., Cheng, Z.G., He, C.Y., 2002a. Tremendous change of the earth surface system and tectonic setting of salt-lake formation in Yuncheng Basin since 7.1 Ma. Sci. China Ser. D: Earth. Sci. 45, 110–122. https://doi.org/10.3969/j.issn.1674-7240.2000.04.012.

Wang, S.B., Jiang, F.C., Wu, X.H., Wang, S.M., Tian, G.Q., Xue, B., Zheng, H.B., 1999. A study on the age of Sanmen Group in Sanmenxia area. J. Geomech. 5, 57–65 (in Chinese with English abstract). https://doi.org/10.3969/j.issn.1006-6616.1999.04.007.

Wang, S.B., Wu, X.H., Jiang, F.C., Tian, G.Q., Liu, K., 2000. Two loess profiles in Pinglu, shanxi and corresponding paleoclimatic reconstruction. J. Geomech. 6, 27–36 (in Chinese with English abstract). https://doi.org/10.3969/j.issn.1006-6616.2000.04.004.

Wang, S.M., Wu, X.H., Zhang, Z.K., Jiang, F.C., Xue, B., Tong, G.B., Tian, G.Q., 2002b. Sedimentary records of environmental evolution in the Sanmen Lake Basin and the Yellow River running through the Sanmenxia Gorge eastward into the sea. Sci. China Ser. D: Earth. Sci. 45, 595–608. https://doi.org/10.3969/j.issn.1674-7313.2002.07.002.

Wang, X.S., Løvlie, R., Yang, Z.Y., Pei, J.L., Zhao, Z.Z., Sun, Z.M., 2005. Remagnetization of Quaternary eolian deposits: a case study from SE Chinese Loess Plateau. Geochem. Geophys. Geosyst. 6, Q06H18. https://doi.org/10.1029/2004GC000901.

Wang, Z.X., Liang, M.Y., Sun, Y.Q., Dai, G.W., 2017. Cenozoic tectonic and geomorphic evolution of the Longxi region in northeastern Tibetan Plateau interpreted from detrital zircon. Sci. China Earth Sci. 60, 256–267.

https://doi.org/10.1007/s11430-016-5247-9.

Warren, J.K., 2010. Evaporites through time: Tectonic, climatic and eustatic controls in marine and nonmarine deposits. Earth-Sci. Rev. 98, 217–268. https://doi.org/10.1016/j.earscirev.2009.11.004.

Wu, X.H., Jiang, F.C., Wang, S.B., Xue, B., 1998. Study on the event of Yellow River passing through Sanmen Gorge. Quat. Sci. 18, 188 (in Chinese with English abstract). https://doi.org/10.3321/j.issn:1001-7410.1998.02.016.

Xia, Z.K., 1992. Underwater loess and paleaclimate. Acta Geogr. Sin. 47, 58–65 (in Chinese with English abstract). https://doi.org/10.3321/j.issn:0375-5444.1992.01.008.

Xiao, G., Sun, Y., Yang, J., Yin, Q., Dupont-Nivet, G., Licht, A., Kehew, A.E., Hu, Y., Geng, J., Dai, G., Zhao, Q., Wu, Z., 2020. Early Pleistocene integration of the Yellow River I: Detrital-zircon evidence from the North China Plain. Palaeogeogr. Palaeoclimatol. Palaeoecol. 546, 109691. https://doi.org/10.1016/j.palaeo.2020.109691.

Xiong, J., Li, Y., Zhong, Y., Si, S., Lei, J., Xin, W., Hu, X., Yao, Y., 2017. Paleomagnetic age of the Tangxian planation surface, northwestern Zhongtiao Shan of the Shanxi Graben System, North China. Geomorphology 283, 17–31. http://dx.doi.org/10.1016/j.geomorph.2017.01.020.

Xiong, J., Li, Y., Zheng, W., Zhang, P., Lei, J., Zhong, Y., Hu, X., Li, Z., Gong, Z., Li, T., Zhang, Y., Xu, B., Tian, Q., Xin, W., Ren, X., Yao, Y., 2018. Climatically driven formation of the Tangxian planation surface in North China: An example from northwestern Zhongtiao Shan of the Shanxi Graben System. Lithosphere 10, 530–544. https://doi.org/10.1130/L720.1.

Xu, Y., Tang, Y., Pan, F., Li, J., Zhang, R., Yue, L., 2019. Palaeomagnetic chronolgy and its tectonic implications of the red clay in the Wujiamao section in west piedmont of the Lüliang Mountains. Quat. Sci. 39, 328–338 (in Chinese with English abstract). http://www.dsjyj.com.cn/CN/Y2019/V39/I2/328.

Xue, X.X., 1981. An early Pleistocene mammalian fauna and the strdtohorizon in Weinan, Shaanxi Province. Vertebr. PalAsiatica. 19, 35–44 (in Chinese with English abstract).

Yan, J.Y., Hu, J.M., Gong, W.B., Liu, X.B., Yin, Y.G., Tan, C., 2020. Late Cenozoic magnetostratigraphy of the Yuncheng Basin, central North China Craton and its tectonic implications. Geol. J. 55, 7415–7428. https://doi.org/10.1002/gj.3744.

Yao, Z.Q., Shi, X.F., Qiao, S.Q., Liu, Q.S., Kandasamy, S., Liu, J.X., Liu, Y.G., Liu, J.H., Fang, X.S., Gao, J.J., Dou, Y.G., 2017. Persistent effects of the Yellow River on the Chinese marginal seas began at least ~880 ka ago. Sci. Rep. 7: 2827. https://doi.org/10.1038/s41598-017-03140-x.

Yu, Q.H., Xing, L.S., Cao, Z.Y., 1982. A tentative discussion on paleomagnetism data from two boreholes drilled in Wugong and Xianyang Counties, Shaanxi Province. J. Geomech. 2, 107–115 (in Chinese with English abstract).

Yuan, F., 1986. Discovery of ostracods from the Sanmen Series and its significance. Acta Micropalaeontol. Sin. 3, 161–166 (in Chinese with English abstract).

Yue, L.P., 1996. Depositional ralation between the loess, red clay and sedimtation of the lake basin in the Loess Plateau. Acta Sedimentol. Sin. 14, 148–153 (in Chinese with English abstract).

Zhang, J., Wan, S.M., Clift, P.D., Huang, J., Yu, Z.J., Zhang, K.D., Mei, X., Liu, J., Han, Z.Y., Nan, Q.Y., Zhao, D.B., Li, A.C., Chen, L.H., Zheng, H.B., Yang, S.Y., Li, T.G., Zhang, X.H., 2019. History of Yellow River and Yangtze River delivering sediment to the Yellow Sea since 3.5 Ma: Tectonic or climate forcing? Quat. Sci. Rev. 216, 74–88. https://doi.org/10.1016/j.quascirev.2019.06.002.

Zhang, Y.Q., Mercier, J.L., Vergely, P., 1998. Extension in the graben systems around the Ordos (China), and its contribution to the extrusion tectonics of south China with respect to Gobi-Mongolia. Tectonophysics 285, 41–75. https://doi.org/10.1016/S0040-1951(97)00170-4.

Zhao, Z.Z., Wu, X.H., Jiang, F.C., Xiao, H.G., Wang, S.B., Tian, G.Q., Liu, K., Yin, W.D., Xue, B., Wang, S.M., 2000. The loess stratigraphy in Sanmenxia area. J. Geomech. 6, 19–26 (in Chinese with English abstract). https://doi.org/10.3969/j.issn.1006-6616.2000.04.003.

Zheng, H.B., Huang, X.T., Ji, J.L., Liu, R., Zeng, Q.Y., Jiang, F.C., 2007. Ultra-high rates of loess sedimentation at Zhengzhou since Stage 7: Implication for the Yellow River erosion of the Sanmen Gorge. Geomorphology 85, 131–142. https://doi.org/10.1016/j.geomorph.2006.03.014.

Zhu, D.G., Meng, X.G., Shao, Z.G., Lei, W.Z., Wang, J., Han, J.E., Yu, J., Lv, R.P., Wang, Y., 2008. Revision and classification of Paleogene fluvial-lacustrine strata in the Pinglu area, Shanxi. Geol. in China. 35, 656–669 (in Chinese with English abstract). https://doi.org/10.3969/j.issn.1000-3657.2008.04.010.

Zhu, Z.Y., 1989. The formation of river terraces and evolutionof drainage system in the middle Yellow River. Acta Geogr. Sin. 44, 429–440 (in Chinese with English abstract). https://doi.org/10.3321/j.issn:0375-5444.1989.04.007.

Figure Captions:

Fig. 1. Map of the main Yellow River course and the basins on its passage. The Upper

(U), Middle (M), and Lower (L) Reaches of the Yellow River are divided by red bold lines. The location of Fig. 2a is also indicated.

Fig. 2. (a) Map of the Fenwei Basin, and its fault system (from Deng et al., 2003) and the locations of the Weihe Subbasin (WHB), Sanmenxia Subbasin (SMB), Yuncheng Subbasin (YCB), and Linfen Subbasin (LFB). The black numbers in red dots show the sites of published sections/boreholes referenced in the text: (1) Wang et al. (1999); (2) He et al. (1984); (3) Wang et al. (2005) and Zhao et al. (2000); (4) Kong et al. (2013); (5–7) Wang et al. (2002a); (8) Yan et al. (2020); (9–10) Li et al. (2004); (11) Qiu et al. (2018); (12) Rits et al. (2016); (13) Han et al. (1997); (14) Ge et al. (1991); (15) Yue (1996); (16) Sun et al. (1988); (17–18) Yu et al. (1982); and (19) Tan et al. (2011). (b) Geologic cross section of the Sanmenxia and Yuncheng Subbasins (from Han et al., 2002).

Fig. 3. The Cenozoic strata in the Sanmenxia Sub-basin. (a) The loess-paleosol sequences in the Guanjiawo subsection. (b) The loess-paleosol sequences in the Hougou subsection. The boundary between the Sanmen Formation and the loess-paleosol sequences is also showed. (c) The boundary between the upper and lower Sanmen Formation in the Hougou subsection. The lower Sanmen Formation is characterized by interbed pale yellow siltstone and green-grayish calcareous mudstone. (d) The boundary between the Sanmen and Youhe Formations. The Youhe Formation is characterized by pale yellow huge-thick lenticular sandstone intercalated with green-

grayish calcareous mudstone. (e) The outcrop in the Bangou village (~4 km to the west of Huangdigou section). The Sanmen Formation and lower Pleistocene loess are exposed in this profile. (f) The Youhe Formation in the upper part of the Huangdigou section, characterized by pale yellow huge-thick lenticular sandstone intercalated with green-grayish calcareous mudstone. (g) The Bahe Formation in the lower part of the Huangdigou section. (h) The Paleogene Pinglu Group exposed near the Sanmenxia reservoir. The red dot line in (a-d) shows where the samples were taken.

Fig. 4. Temperature-dependence of magnetic susceptibility (χ-T) curves of representative samples from different depths of the Zhangcun section. Solid red and dashed blue lines represent heating and cooling curves, respectively.

Fig. 5. Isothermal remanent magnetization (IRM) acquisition curves for representative samples from different depths of the Zhangcun section.

Fig. 6. FORC diagrams for representative samples from different depths of the Zhangcun section.

Fig. 7. Orthogonal (Zijderveld) vector plots of representative specimens from the Zhangcun section (a-f). The solid and open circles represent vector end-points projected onto the horizontal and vertical planes, respectively. NRM is the natural remanent magnetization before demagnetization.

Fig. 8. Lithostratigraphy, magnetic susceptibility, and magnetostratigraphy of the (a) Zhangcun and (b) Caocun (Wang et al., 2005; Zhao et al., 2000) sections, with the correlation to the GPTS2012 (Ogg, 2012). Normal polarity intervals labeled N with a number. The dashed lines in Fig. 8a represent the average values of magnetic susceptibility for different intervals.

Fig. 9. Re-interpretation of the magnetostratigraphic study of the Huangdigou section by Wang et al. (1999). Note that the Huangdigou section contains a hiatus between ~2.6 and 0.15 Ma.

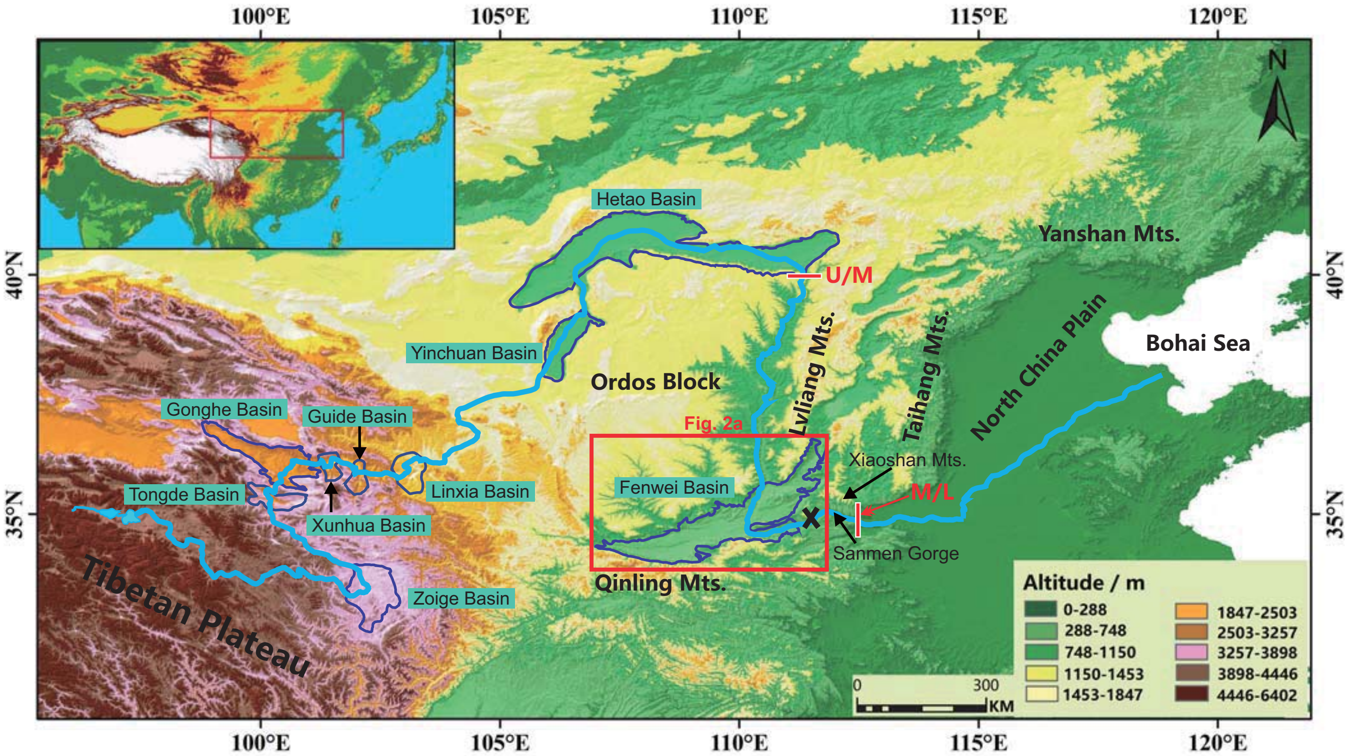

100°E
105°E
110°E
115°E
120°E
40°N
35°N
N
Hetao Basin
U/M
Yanshan Mts.
Yinchuan Basin
Ordos Block
Lvliang Mts.
Taihang Mts.
North China Plain
Bohai Sea
Gonghe Basin
Guide Basin
Fig. 2a
Xiaoshan Mts.
Tongde Basin
Linxia Basin
Fenwei Basin
M/L
Xunhua Basin
Sanmen Gorge
Tibetan Plateau
Zoige Basin
Qinling Mts.
Altitude / m
0-288
288-748
748-1150
1150-1453
1453-1847
1847-2503
2503-3257
3257-3898
3898-4446
4446-6402
0
300
KM

Figure 1

Figure 2

Click here to access/download;Figure;Figure 2.pdf

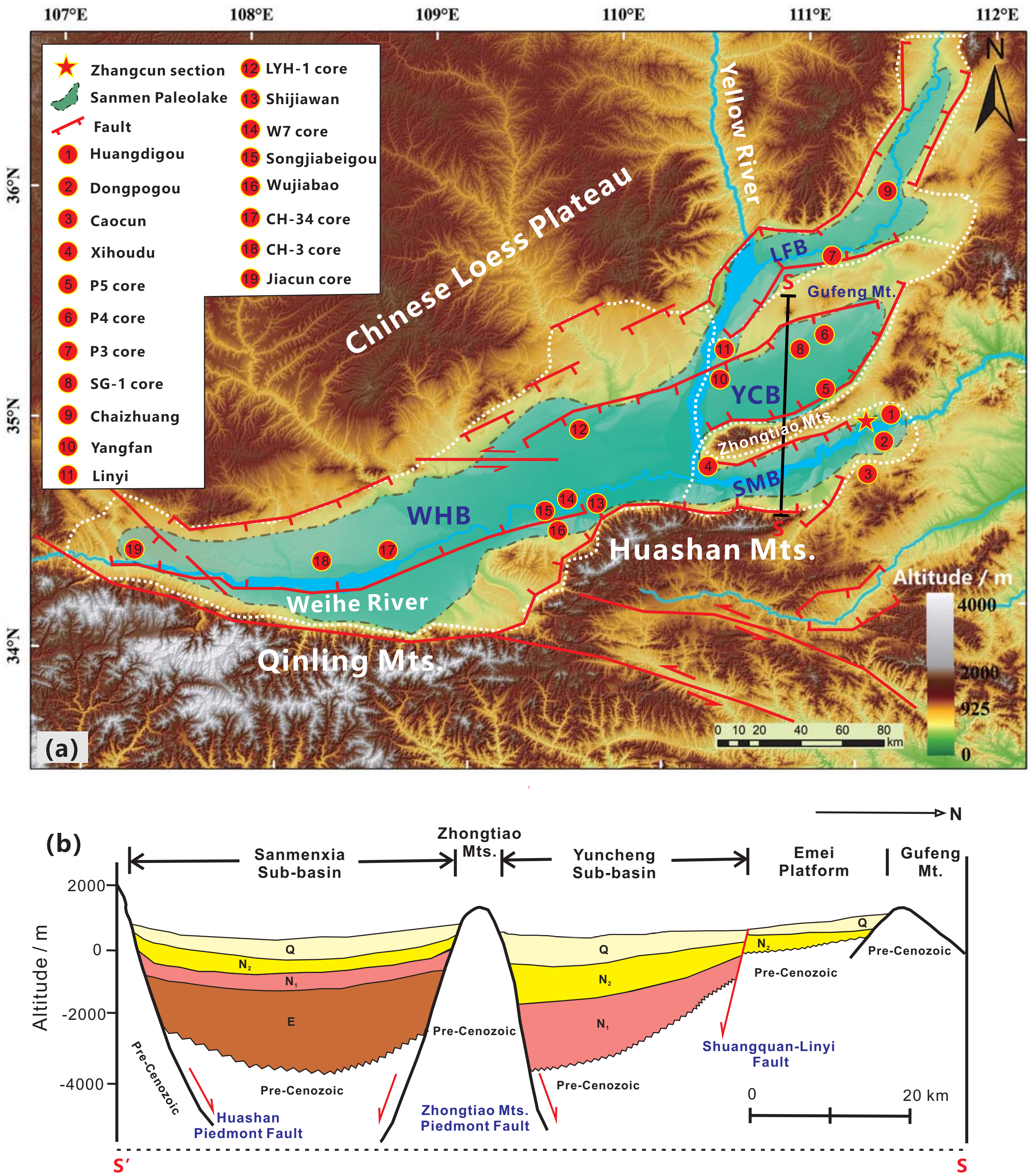

Figure 2

Figure 3

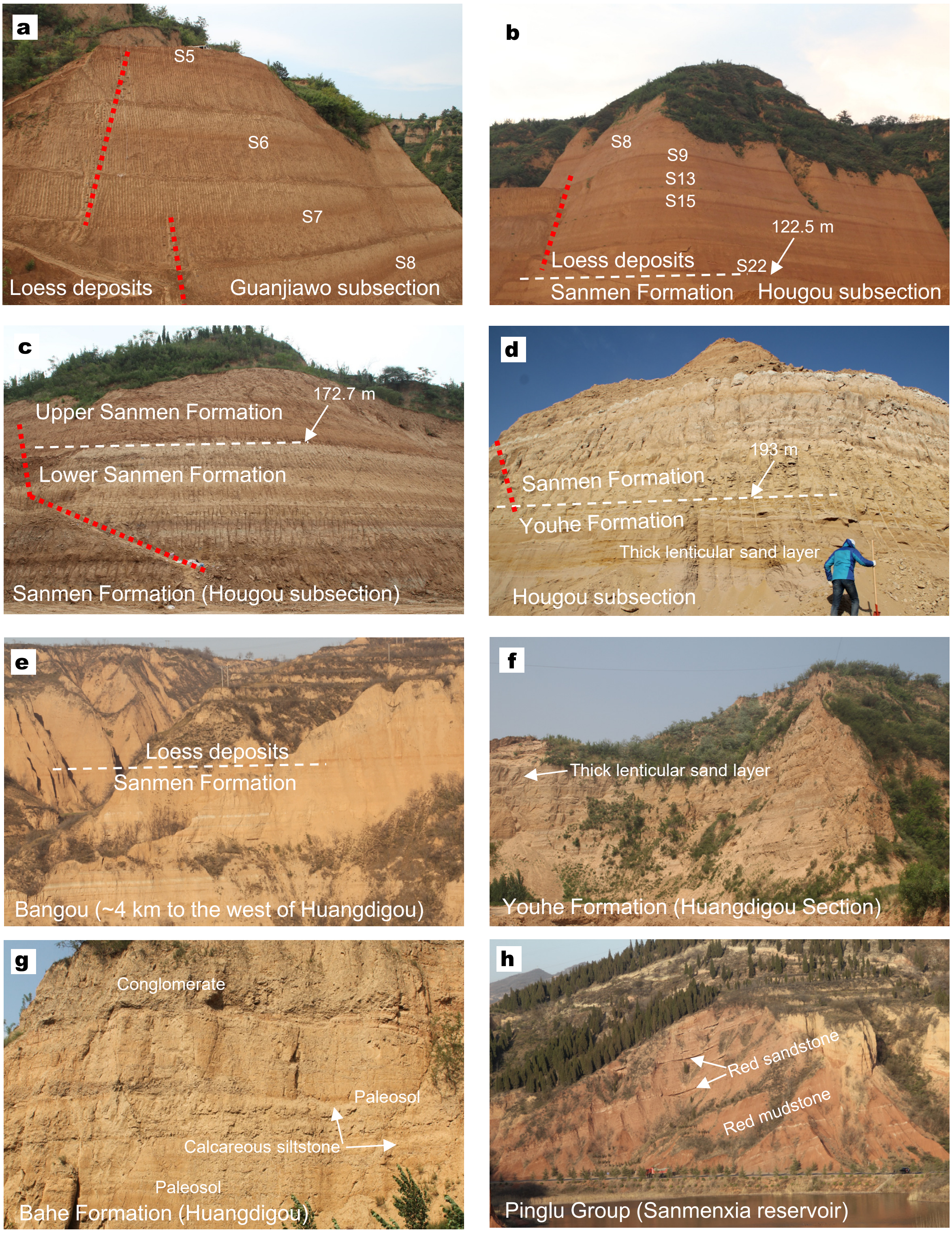

Figure 3

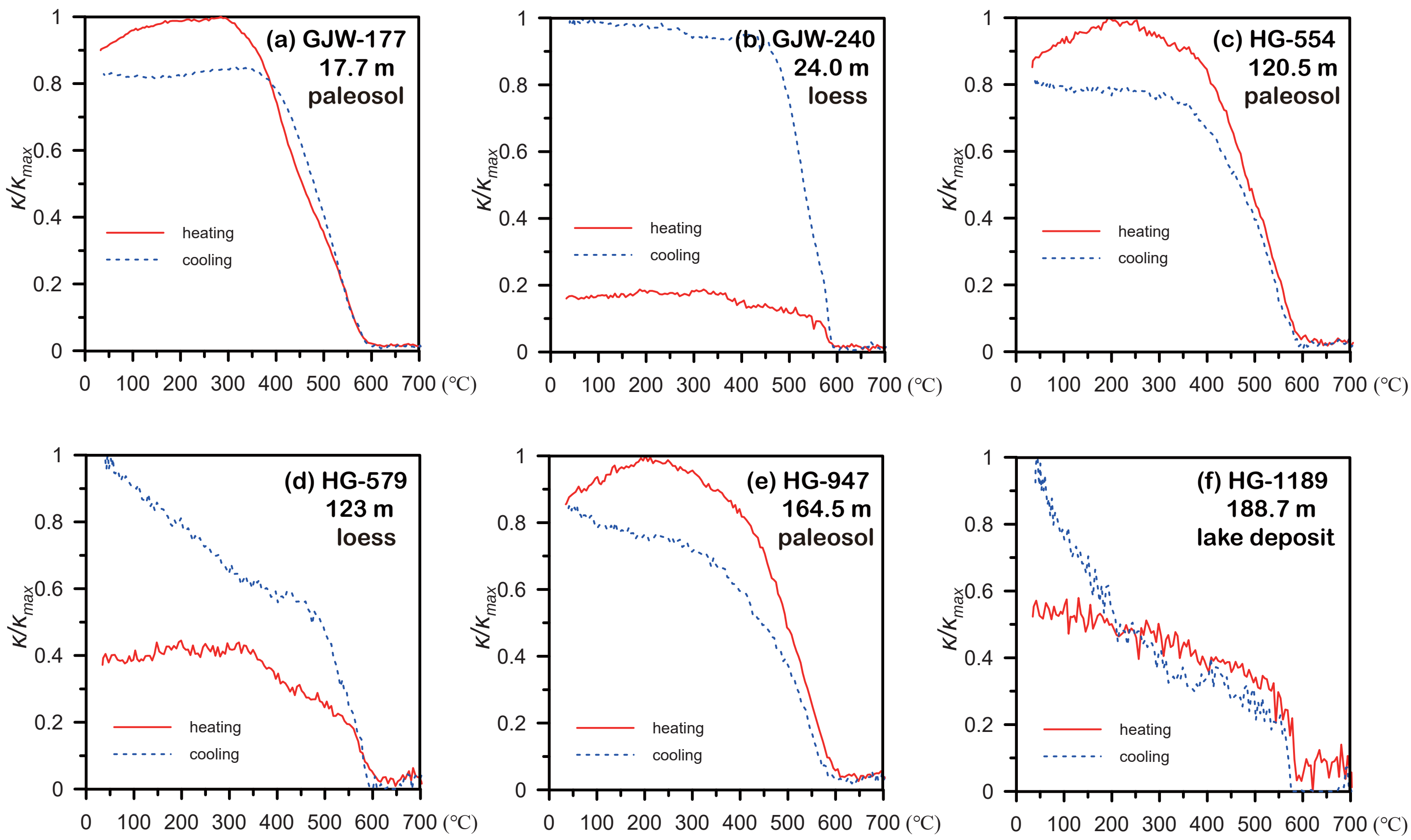
(a) GJW-177
17.7 m
paleosol
(b) GJW-240
24.0 m
loess
(c) HG-554
120.5 m
paleosol
(d) HG-579
123 m
loess
(e) HG-947
164.5 m
paleosol
(f) HG-1189
188.7 m
lake deposit
heating
cooling
κ/κmax
0 100 200 300 400 500 600 700 (℃)
0 0.2 0.4 0.6 0.8 1

Figure 4

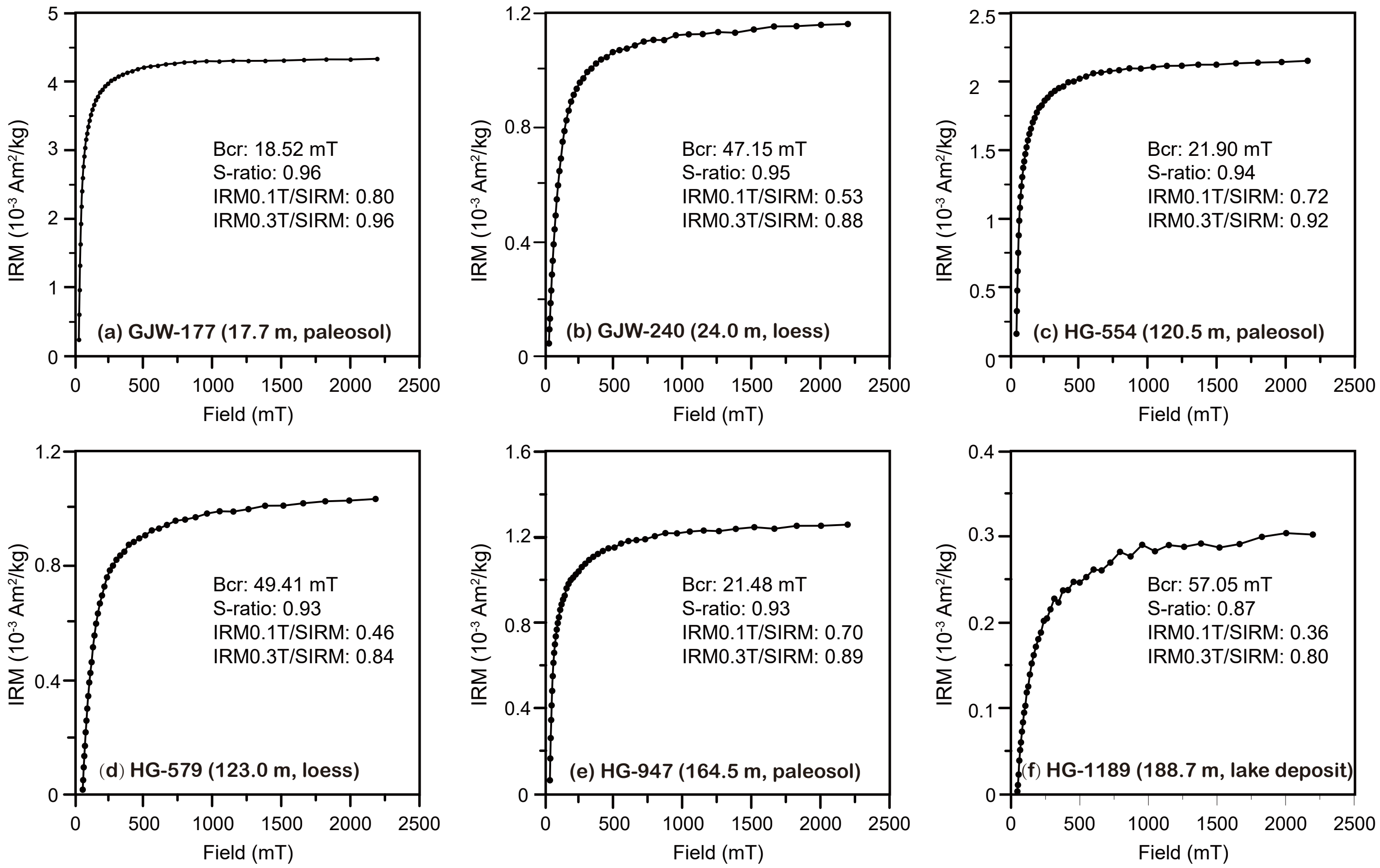

IRM (10-3 Am2/kg)
Field (mT)
Bcr: 18.52 mT
S-ratio: 0.96
IRM0.1T/SIRM: 0.80
IRM0.3T/SIRM: 0.96
(a) GJW-177 (17.7 m, paleosol)
Bcr: 47.15 mT
S-ratio: 0.95
IRM0.1T/SIRM: 0.53
IRM0.3T/SIRM: 0.88
(b) GJW-240 (24.0 m, loess)
Bcr: 21.90 mT
S-ratio: 0.94
IRM0.1T/SIRM: 0.72
IRM0.3T/SIRM: 0.92
(c) HG-554 (120.5 m, paleosol)
Bcr: 49.41 mT
S-ratio: 0.93
IRM0.1T/SIRM: 0.46
IRM0.3T/SIRM: 0.84
(d) HG-579 (123.0 m, loess)
Bcr: 21.48 mT
S-ratio: 0.93
IRM0.1T/SIRM: 0.70
IRM0.3T/SIRM: 0.89
(e) HG-947 (164.5 m, paleosol)
Bcr: 57.05 mT
S-ratio: 0.87
IRM0.1T/SIRM: 0.36
IRM0.3T/SIRM: 0.80
(f) HG-1189 (188.7 m, lake deposit)

Figure 5

Figure 6 Click here to access/download;Figure;Figure 6.pdf

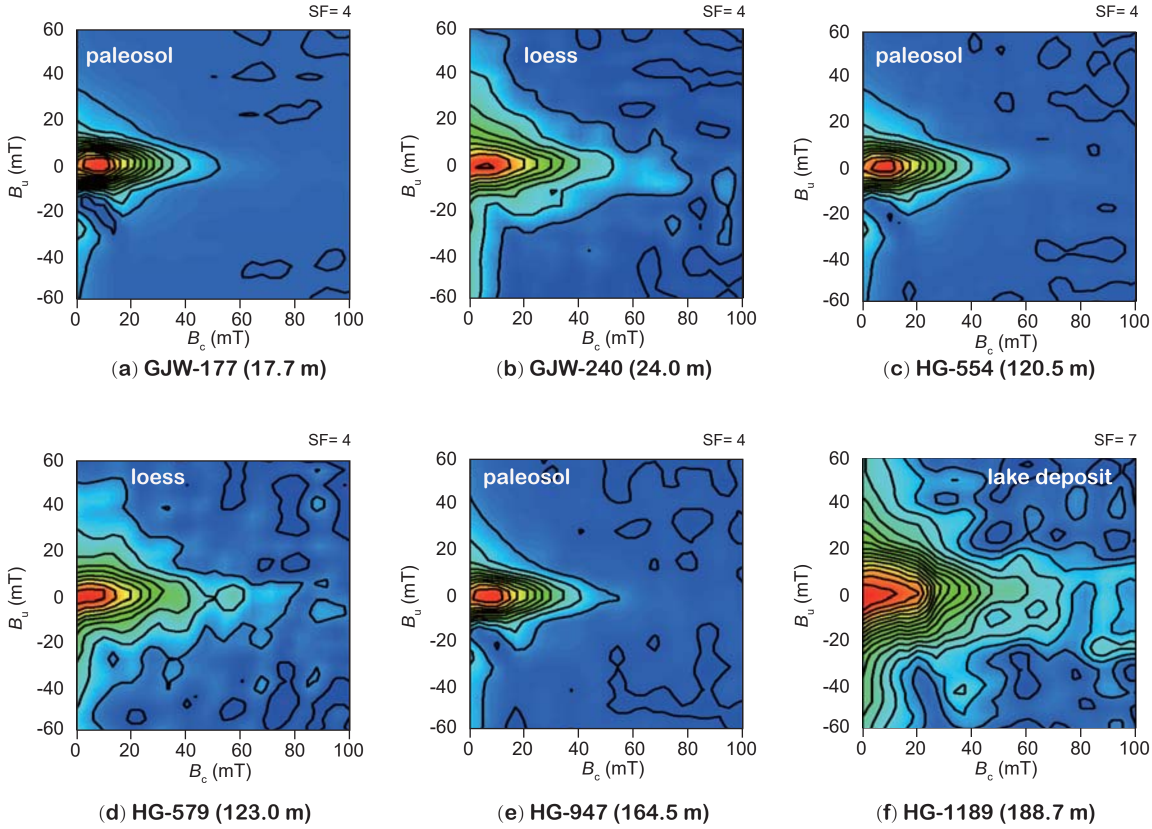

Figure 6

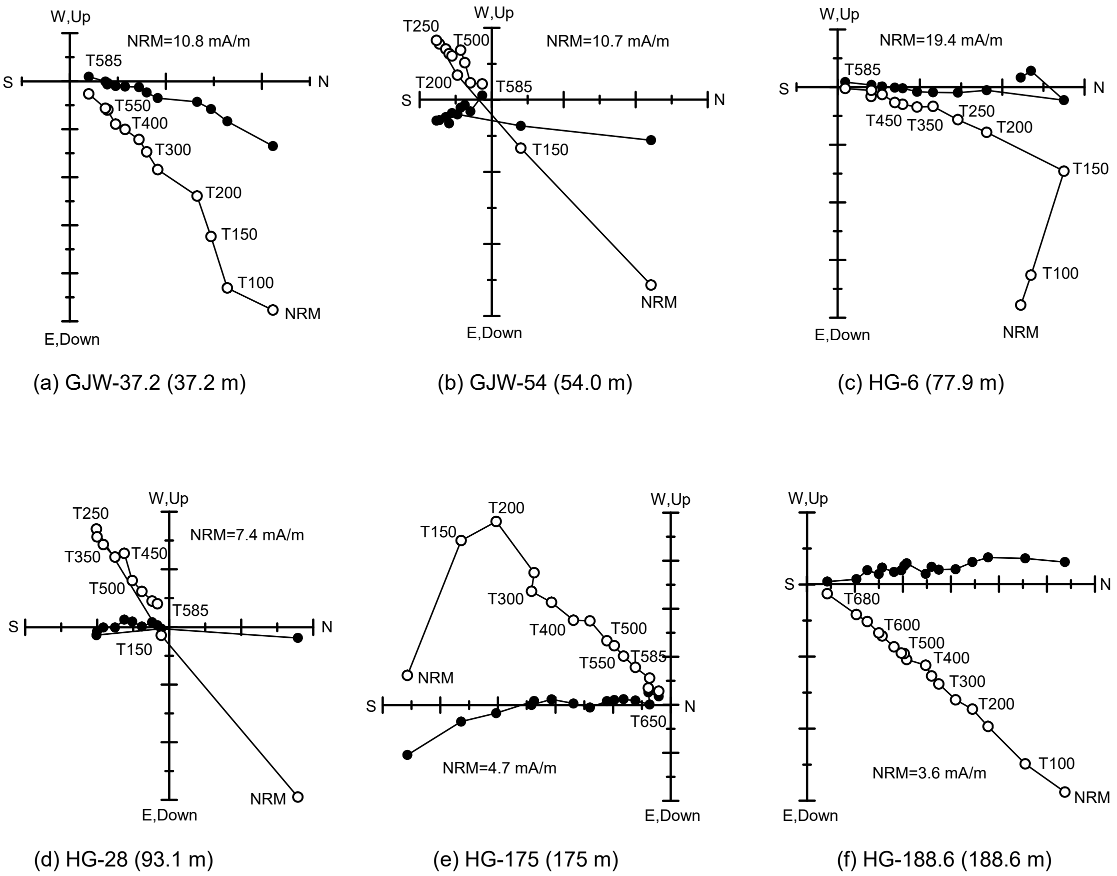
W,Up
NRM=10.8 mA/m
T585
S
N
T550
T400
T300
T200
T150
T100
NRM
E,Down
(a) GJW-37.2 (37.2 m)
T250
T500
W,Up
NRM=10.7 mA/m
T200
T585
T150
NRM
E,Down
(b) GJW-54 (54.0 m)
W,Up
NRM=19.4 mA/m
T585
T450
T350
T250
T200
T150
T100
NRM
E,Down
(c) HG-6 (77.9 m)
T250
W,Up
NRM=7.4 mA/m
T350
T450
T500
T585
T150
NRM
E,Down
(d) HG-28 (93.1 m)
T200
W,Up
T150
T300
T400
T500
T550
T585
NRM
T650
NRM=4.7 mA/m
E,Down
(e) HG-175 (175 m)
W,Up
T680
T600
T500
T400
T300
T200
T100
NRM
NRM=3.6 mA/m
E,Down
(f) HG-188.6 (188.6 m)

Figure 7

Figure 8 Click here to access/download;Figure;Figure 8R.pdf

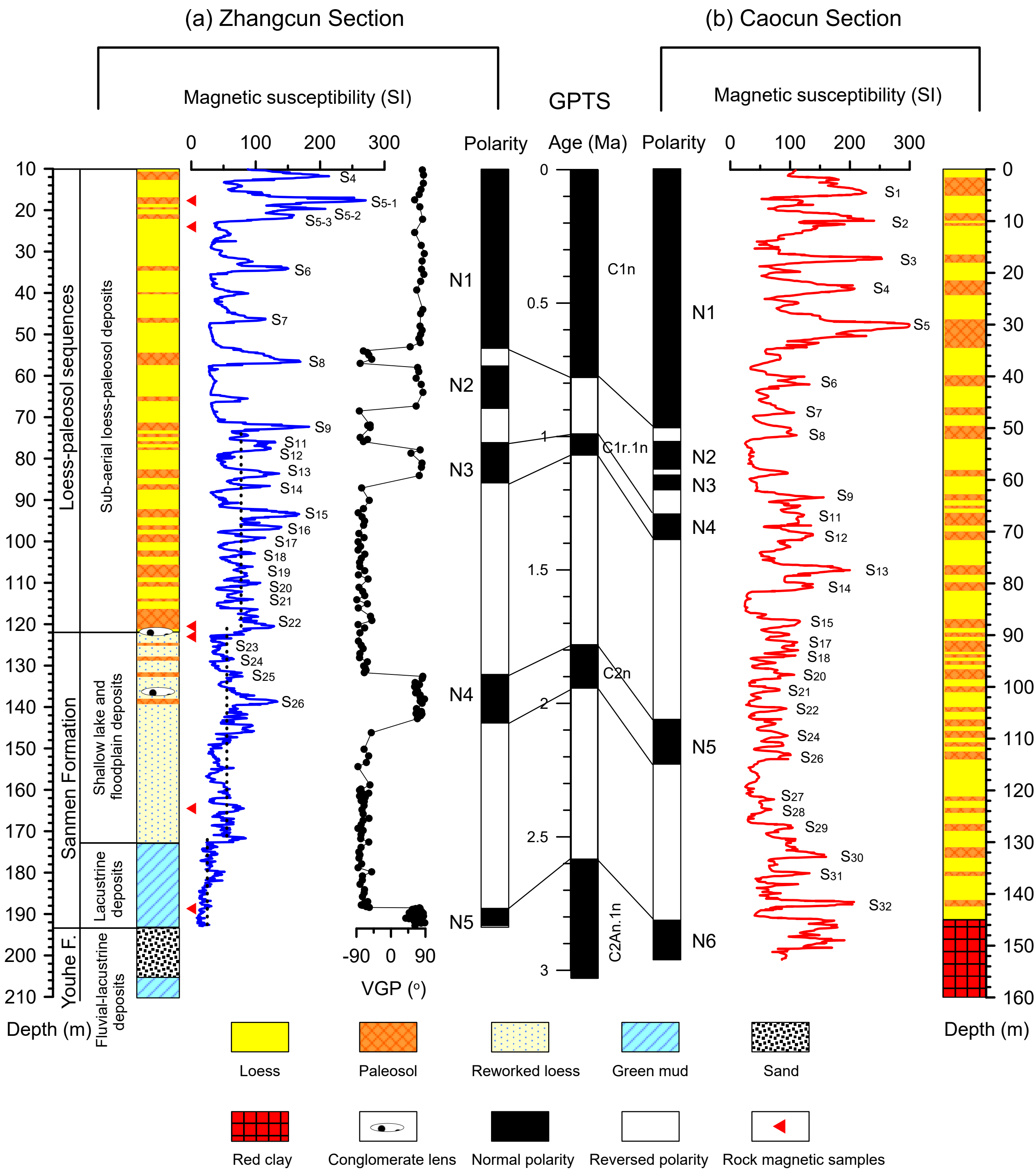

Figure 8

Figure 9

Click here to access/download;Figure;Figure 9.pdf

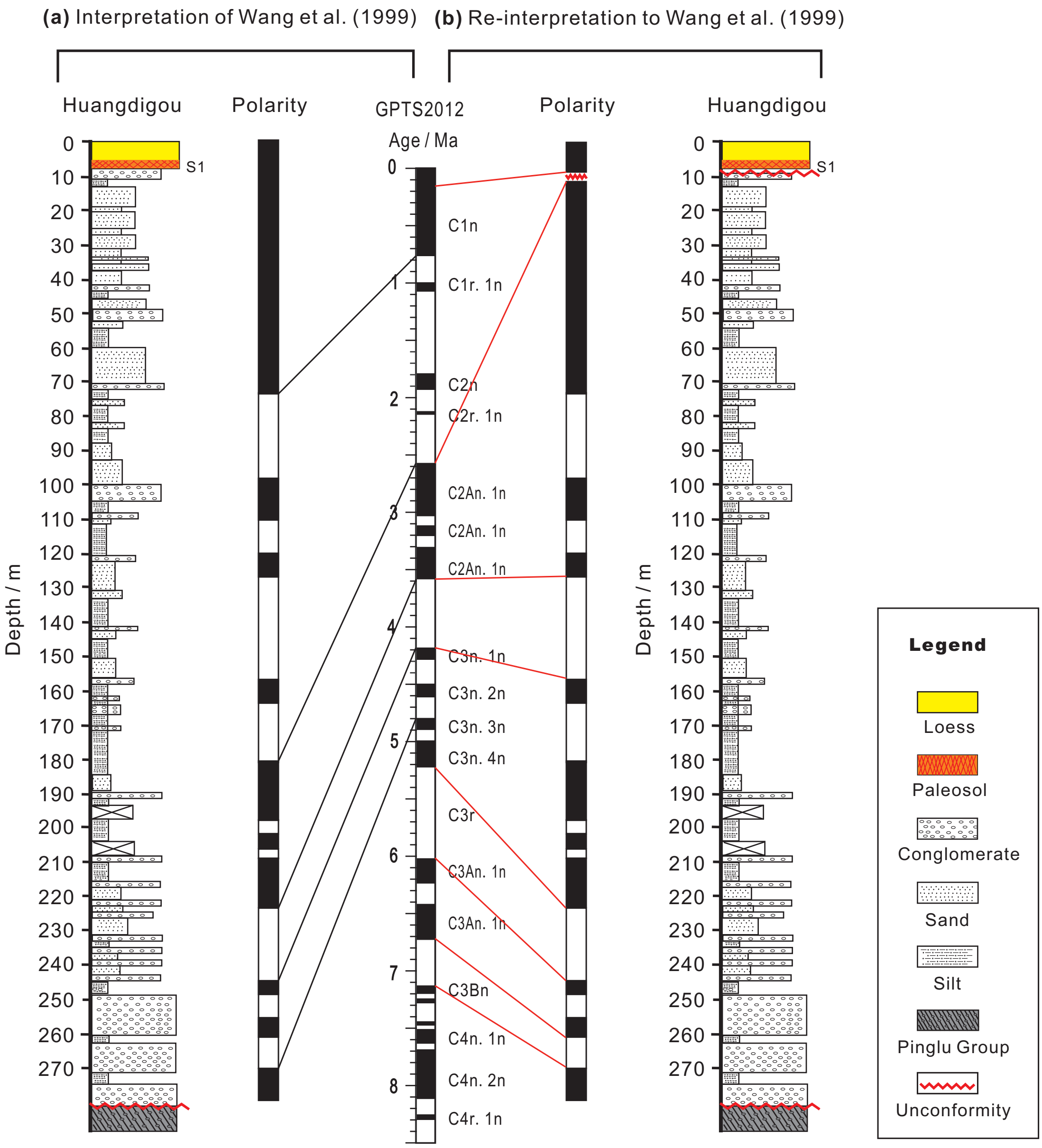

Figure 9